Korean J. Chem. Eng., 39(6), 1496-1506 (2022)
DOI: 10.1007/s11814-022-1084-5

pISSN: 0256-1115
eISSN: 1975-7220

Preparation and characterization of room-temperature chemically expanded graphite: Application for cationic dye removal

Mahnaz Movafaghi Ardestani*, Shokouh Mahpishanian, Bahar Forouzesh Rad*, Mehran Janmohammadi***, and Majid Baghdadi*,†**

*School of Environment, College of Engineering, University of Tehran, Tehran, Iran
**Department of Chemical and Materials Engineering, New Mexico State University, Las Cruces, 88003, United States
***Department of Civil Engineering, Monash University, Melbourne, VIC 3800, Australia
(*Received 16 August 2021 • Revised 25 January 2022 • Accepted 3 February 2022*)

Abstract−A facile, effective, and eco-friendly process was developed for the preparation of chemically expanded graphite (CEG) under ambient conditions using natural flake graphite as raw material, potassium permanganate ($KMnO_4$) as an oxidative intercalating agent, and hydrogen peroxide (H_2O_2) as the reactive species. The results showed that the CEG had an interconnected and highly porous structure, and some oxygen-containing groups were grafted on the graphite layer by the oxidation-intercalation process. The absence of the graphite diffraction peak at 26° in the XRD pattern of expanded graphite (EG) indicates that the intercalation and expansion processes were complete, and most of the starting graphite layers were converted into the graphene sheets. The sulfuric acid concentration was the most effective parameter on the expansion, and the maximum expansion occurred at a sulfuric acid concentration of 77.5%. The other optimum preparation conditions were obtained at 1.5 g of $KMnO_4$ and 30 mL of H_2O_2 30%. Under the optimal condition, the developed room-temperature liquid-phase intercalation and expansion processes led to an expansion volume of up to 250 times. The potential application of the as-prepared CEG in environmental clean-up was evaluated by adsorptive removal of methylene blue (MB) from the aqueous solution. The kinetic studies exhibited that the MB adsorption onto the CEG followed a pseudo-second-order kinetic model. Equilibrium data were fitted well with the Langmuir model with a maximum adsorption capacity of 399.08 mg g^{-1}. The findings indicate that the CEG would be potentially applicable in water purification.

Keywords: Expansion, Intercalation, Graphite, Graphene, Adsorption, Water Treatment

INTRODUCTION

Graphite has a crystal layered structure with a weak van der Waals force bonding the layers. Because of the weak force between the layers, intercalating the layers with a wide range of atoms can provide expanded graphite (EG) with incredibly higher pore size compared to graphite [1].

EG can be obtained by the expansion of graphite layers along the c-axis [2]. However, the van der Waals forces between the adjacent layers prevent the c-axis exfoliation of graphite. Therefore, for the successful expansion of graphite, it needs to overcome the van der Waals bonds between the layers by physical or chemical methods. The van der Waals forces can be weakened by inserting atomic or molecular non-carbonaceous chemical species between graphite layers [3]. Using high temperature or chemical reactions, the decomposition of the inserted compounds between layers produces a large volume of gas, resulting in a large force between the layers greater than the van der Waals binding forces that push away the layers along the c-axis [4]. This would result in the expansion of the intercalated graphite (also known as graphite intercalation compound or expandable graphite) to hundreds of times of its initial volume and formation of a porous worm-like filament. The resulting material is called expanded graphite, which has a different structure as well as properties than those of flake graphite, such as high specific surface area and good adsorption ability [5-7]. EG has been successfully applied to remove various organic and inorganic compounds, such as pesticides [8,9], oils [10,11], heavy metals [12-15], and dyes [16-18].

The expansion process of graphite can be achieved by various strategies, such as thermal, chemical, and electrochemical processes [19,20]. Thermal expansion mainly occurs by the release of gas within the interlayers at high temperatures, produced by the sudden volatilization of intercalant species inserted between adjacent layers, causing each region to expand like a balloon [21]. The main drawback of this process is the inhomogeneous gas shock to graphite layers, which results in the formation of multilayer stacked structures.

Electrochemical expansion is a highly efficient and environmentally friendly procedure for the production of EG. This process is based on graphite anodic polarization (formation of carbon macrocations) and diffusion of intercalant substances into inter-layer spaces [22-24]. However, the generation of radicals during the water electrolysis is a major problem since these radicals can attack the lattice of sp^2-bonded carbon atoms, resulting in the formation of defects in the structure [25].

Chemical expansion is another way to prepare the EG [26]. The

†To whom correspondence should be addressed.
E-mail: m.baghdadi@ut.ac.ir

gas evolution between the layers originating from the chemical reaction of inserted intercalants with reactive substance is important for the graphite expansion in this route. In the production of chemically expanded graphite (CEG), reactant types and their content affect intensively the volume of expansion as well as the structure. Various types of intercalation compounds, such as sulfuric acid [27,28], peroxodisulfuric acid [29], nitric acid [30,31], acetic acid [32], perchloric acid [33,34], ferric chloride [35], barium ferrite [36], and ammonium persulfate [37], have been used to prepare expandable graphite materials. However, the toxicity of precursors in some cases and uneconomic process conditions such as the need for applying high temperatures or using other co-intercalant/oxidant species can limit their widespread application for the preparation of CEG materials [4,37,38]. A novel room-temperature chemical expansion method of graphite using CrO_3 as intercalant and H_2O_2 as reactive species was developed in 2016 by Lin et al. [20] to prepare high-quality EG. However, this method involves the utilization of the toxic CrO_3 and subsequent generation of environmental pollutant chromium ions during the expansion process. Therefore, it is essential to develop new methods for highly efficient mass production of CEG with less pollution.

In this study, a simple room-temperature method was developed to produce high-quality CEG. In this method, the CEG is prepared by acidic modification, which can be classified as a sub-category of of chemical expansion, of graphite at ambient temperature using natural flake graphite as raw material, $KMnO_4$ as the intercalant reagent, and H_2O_2 as the reactive species. The impact of effective parameters on the expansion volume was investigated and optimized. The structural change of the graphite during the intercalation/expansion process was investigated with various methods. The potential ability of the as-prepared CEG in water treatment was examined by MB removal from an aqueous solution as a model.

MATERIALS AND METHODS

1. Reagents and Materials

Natural flake graphite (+100 mesh) was obtained from Sigma-Aldrich (St. Louis, MA, USA). Potassium permanganate ($KMnO_4$), Methylene blue (MB, $C_{16}H_{18}N_3SCl$), H_2SO_4 (97%), and H_2O_2 (30%) were purchased from Merck Company (Darmstadt, Germany).

2. Instrumentation

The infrared spectrum was recorded using the KBr pellets on a Spectrum RXI Fourier transform infrared (FTIR) spectrophotometer (PerkinElmer, USA) in the range of 400 to 4,000 cm^{-1}. The surface morphology of materials was investigated using a field emission MIRA3TESCAN-XMU scanning electron microscope (SEM, Czech Republic) at an accelerating voltage of 15 kV. The surface area and pore size of the synthesized material were determined using nitrogen adsorption-desorption analysis with BET-NOVA 2000e (Quantachrome Instruments, USA) at 77 K according to the Brunauer-Emmett-Teller (BET) method. The X-ray diffraction (XRD) patterns were recorded using a PW 1800 X-ray diffractometer (Philips, the Netherlands), equipped with Cu-Kα radiation (λ=0.154056 nm). Raman spectra were recorded using a TEKSAN N1-541 Raman spectrometer (Iran) at an excitation laser beam wavelength of 532 nm. The Malvern Zetasizer 3000 was used to measure zeta potential of the CEG.

3. The Synthesis Procedure of CEG

1.5 g of $KMnO_4$ and 1.0 g of natural flake graphite (+100 mesh) were slowly added to 20 mL of sulfuric acid (77.5%) in a beaker, and the mixture was stirred at room temperature for 90 min. After that, 30 mL of H_2O_2 (30%) was slowly added to the mixture. The mixture was kept at room temperature to complete the expansion of graphite. After 24 hours, the mixture was washed with deionized water several times to remove the residual sulfuric acid and MnO_2 ions. Then, in order to measure the expansion volume, the CEG was poured into a graduated cylinder and its volume was measured. The obtained EG was simply mesh-filtered (100-mesh) and dried at room temperature. The CrO_3 based CEG was synthesized according to the previously reported procedure by Lin et al [20].

4. MB Adsorption Test

MB solution with the initial concentration of 100 $mg \cdot L^{-1}$ was prepared by dissolving a certain amount of MB in deionized water. Then, 0.02 g of EG was transferred to 50 mL of MB solution, and the solution was magnetically stirred for 90 min. After adsorption, the EG was removed and the final concentration of MB was measured by a spectrophotometer at 665 nm. The quantity of MB adsorbed by EG at equilibrium (q_e, $mg \cdot g^{-1}$) was calculated based on the following equation (Eq. (1)):

$$q_e = \frac{(C_i - C_e) \times V}{m} \quad (1)$$

where C_i and C_e are the initial and equilibrium concentrations of MB solution ($mg \cdot L^{-1}$), respectively, V is the volume of MB solution (L) and m is the mass of the CEG (g). For each point, three replicates were done and the average of results was reported.

RESULTS AND DISCUSSION

1. Mechanism of Expansion

The expansion of graphite in the presence of $KMnO_4$, H_2SO_4, and H_2O_2 happens primarily by the evolution of O_2 gas within the interlayer graphite plane. Fig. 1(a) schematically shows the preparation procedure of the CEG. In this process, first, by mixing graphite with $KMnO_4$ and sulfuric acid, the intercalation reaction is achieved by MnO_3^+ ion that further reacts with excess $KMnO_4$ to form Mn_2O_7, which is more reactive than $KMnO_4$ (Eq. (2) and Eq. (3)) [39,40]. The distributed Mn_2O_7 molecules in the interlayer of graphite form a dark green mixture. The intercalation of manganese heptoxide molecules between the graphite layers can weaken the van der Waals forces between them and allow easier exfoliation. However, the intercalation process failed to cause a significant volume expansion for graphite flakes. When H_2O_2 is added to the mixture, the intercalant species (Mn_2O_7 molecules) between the graphite layers react with H_2O_2, which causes release of oxygen gas (Eq. (4)). The large volumes of O_2 gas evolving rapidly have not enough time to escape from the interlayers, and therefore the expansion of intercalated graphite happens. Actually, by the chemical reaction of the adsorbed intercalating agent (Mn_2O_7) on the surface of graphite with H_2O_2, the hydrophobic surface of graphite layers becomes hydrophilic due to the presence of Mn^{2+} ions, which allows

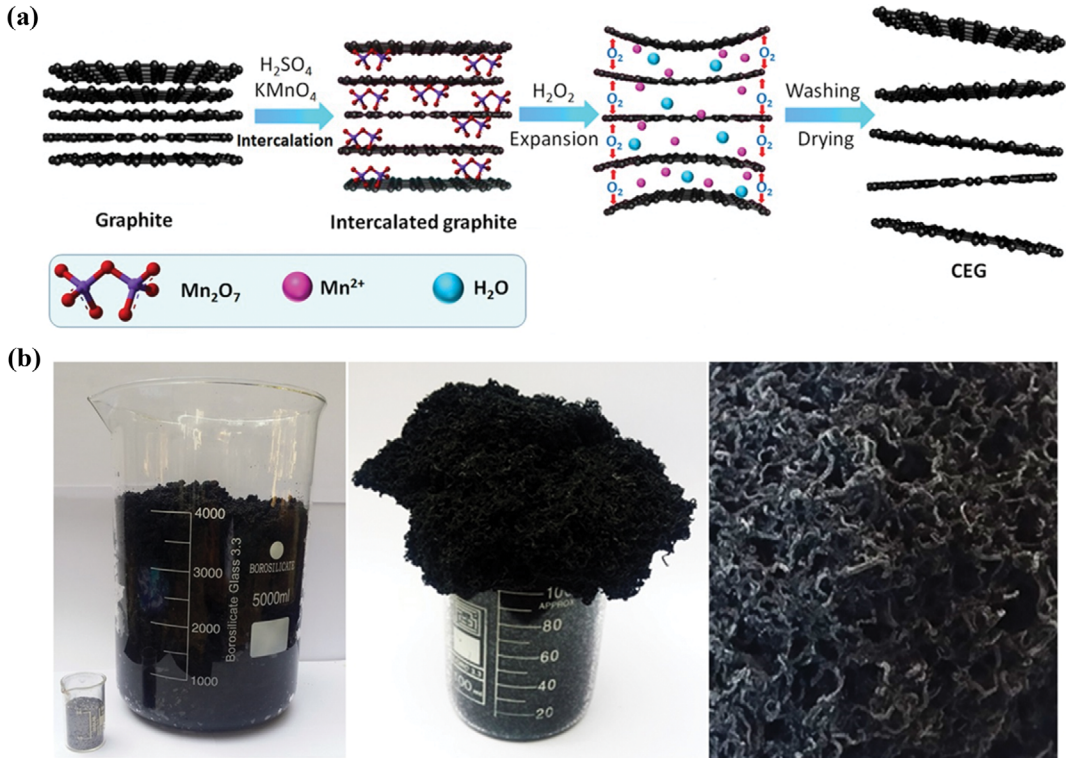

Fig. 1. (a) Schematic representation of the Mn_2O_7 based-chemical expansion process of graphite; (b) digital photos of the as-synthesized CEG.

more H_2O_2 and H_2O molecules to enter the interlayers of graphite and provides better volume expansion. Therefore, the presence of H_2O molecules is also required for the significant expansion of the intercalated graphite. The whole reactions result in the formation of a bulky intertwined black worm-like product attributed to a large expansion of the graphite layers along the c-axis (Fig. 1(b)). The CEG shows a fluffy morphology with an apparent volume of 250 $mL \cdot g^{-1}$ of the starting flake graphite.

$$KMnO_4 + 3H_2SO_4 \rightarrow K^+ + MnO_3^+ + H_3O^+ + 3HSO_4^- \quad (2)$$

$$MnO_3^+ + MnO_4^- \rightarrow Mn_2O_7 \quad (3)$$

$$Mn_2O_7 + H_2O_2 + 4H^+ \rightarrow 2Mn^{2+} + \uparrow 3O_2 + 3H_2O \quad (4)$$

2. Characterization of the CEG

SEM images of the prepared Mn_2O_7-CEG in this study and those of CrO_3-CEG were provided to detect and compare the graphite

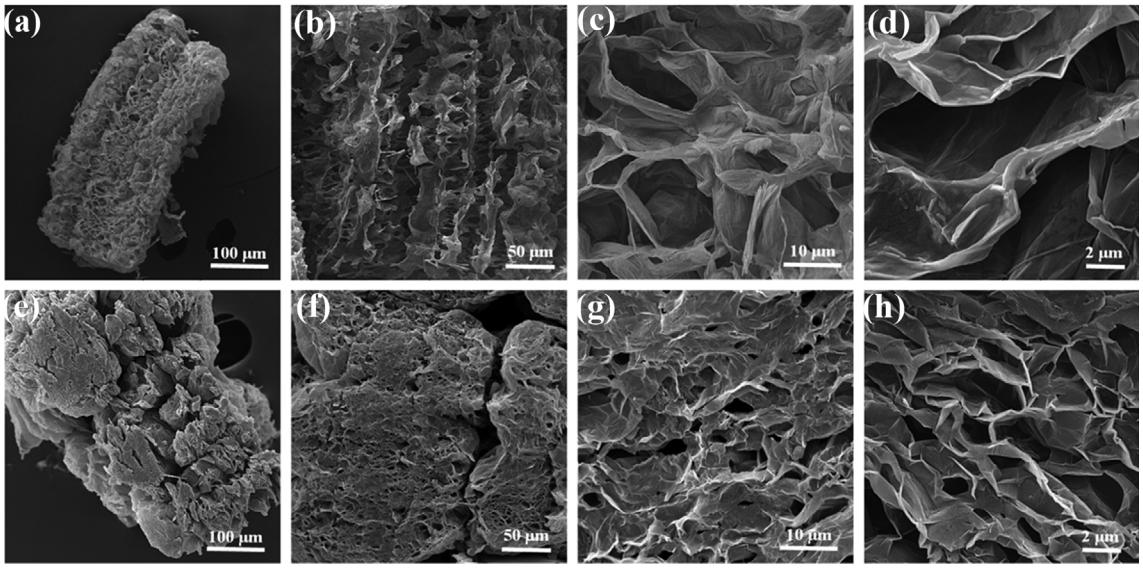

Fig. 2. SEM images of (a)-(d) Mn_2O_7-CEG; and (e)-(h) CrO_3-CEG.

structural change that occurred during the chemical expansion. Moreover, Fig. S1 in the supplementary information shows SEM image of unmodified grafit. EDS analysis of CEG is presented on Table S1 showing the oxygen content of 28.2%, which is a result of relatively oxidation of graphite layers. As shown in Fig. 2(a), the resulting Mn_2O_7 based CEG has a homogeneous and highly porous structure with wrinkled edges and clear marks of bulging and spalling, which is mainly due to the interaction of the intercalation reagent with H_2O_2 solution and generation of a large volume of O_2 gas escaping from the layers which leave behind a highly porous and disrupted region. The magnified images (Fig. 2(b)-(d)) present that many open or semi-open honeycomb pores are formed between the layers during the chemical expansion. This structure is relatively different from that of the CrO_3-CEG (Fig. 2(e)-(h)). For the CrO_3-CEG, some grooves appear in the structure, and the pores are smaller than that of $KMnO_4$-CEG. Therefore, it is expected that the specific surface of Mn_2O_7-CEG would be higher than that of the CrO_3-CEG. However, compared to unmodified graphite (Fig. S1) both $KMnO_4$-CEG and CrO_3-CEG show more porous structure due to interaction of graphite layers.

XRD patterns of graphite and CEG are shown in Fig. 3(a). As is obvious, the flake graphite reveals a sharp characteristic diffraction peak at 2θ=26° (002), indicating a high degree of crystallization in the graphite structure. After entering the intercalant molecules to the interlayers and interacting with hydrogen peroxide, such order structures are significantly decreased, which causes the disappearance of the graphite peak. The absence of the graphite diffraction peak at 26° in the XRD pattern of EG indicates that the intercalation and expansion processes are complete and most of the starting graphite layers have been converted into the graphene sheets. Fig. S2 shows SEM images of unmodified graphite (sideview) and CEG, which can also confirm the conversion of graphite layers to graphene sheets. The appearance of two new broad diffraction peaks in the XRD pattern of the EG at 9.9° and 22° can be attributed to the oxidized and unoxidized regions of the graphene sheets, respectively. In addition, it appears that the intensity of these diffraction peaks was reduced in comparison with the graphite diffraction peak, which can be due to the increased interlayer distances. In fact, the graphite layers were partially oxidized, and intercalation molecules entered graphite interlayers, which resulted in an increase in the graphite layer distance and a decrease in the peak intensity and diffraction angle. The XRD pattern of the CEG in this research was also compared with the same study by Lin et al. that they used CrO_3 as the precursor for graphite expansion (Fig. 3(b)). As mentioned above, no graphite diffraction peak was observed for the $KMnO_4$-CEG, while it can be seen in the XRD pattern of the CrO_3-CEG, which can be discernible due to the existence of a part of graphite structure in the final product.

The structural and electronic properties of as-prepared CEG were analyzed by Raman spectroscopy to explore the ordered and disordered crystal structure (Fig. 3(c)). The D band in the Raman spectrum is related to the disorder-induced mode associated with the sp^3 defect sites or flake edges, while the G band is ascribed to the first-order scattering of the E_2g mode from the in-plane vibration of sp^2 bonded carbon atoms in a graphitic hexagonal lattice. Therefore, the intensity ratio of ID/IG is often used to estimate the amount of disorder in the structure. As shown in Fig. 3(c), the characteristic D and G bands were located at about 1,354 and 1,589 cm^{-1}, respectively, and the ID/IG ratio was 0.72, indicating a relatively high graphitization degree of the CEG and few defects in its structure. Moreover, it has been reported that high defects in the structure of graphite materials would broaden the G peak [41]. From the spectrum, the G peak of the CEG is quite sharp, confirming that there is a small amount of defects in the structure.

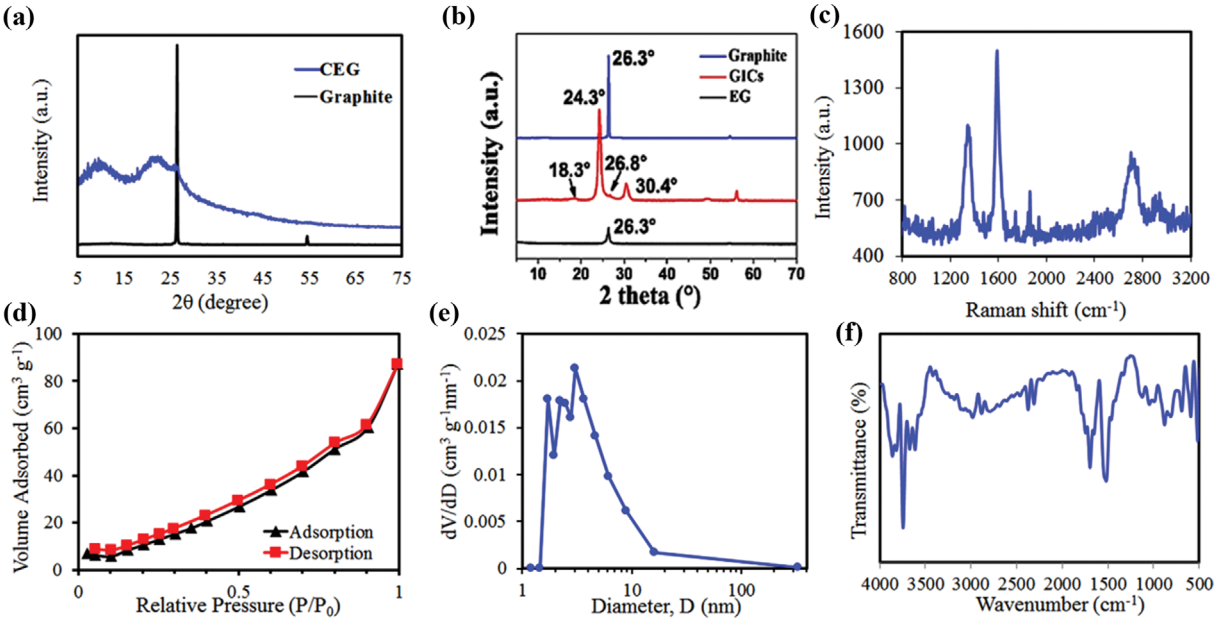

Fig. 3. (a) XRD patterns of graphite and CEG; (b); XRD patterns of graphite, chemically intercalated graphite and CrO_3-CEG (Reprinted with permission from ref [20]); (c) Raman spectrum of the CEG; (d) N_2 adsorption-desorption isotherm of CEG; (e) BJH pore size distribution curve of CEG; (f) FT-IR spectrum of CEG.

Indeed, the Raman spectrum indicates a little oxidized GO-like phase on the surface of the CEG and unchanged graphene inner layers. The broad 2D band centered at about 2,720 cm^{-1} resulting from the out-of-plane vibrational mode and an S3 band at ~2,923 cm^{-1} originating from the combination of the D and G peaks are other indicators for the structure disorder. These results suggest the few-defect feature for the prepared CEG.

The N_2 adsorption-desorption isotherm of CEG and corresponding Barrett-Joyner-Halenda (BJH) pore size distribution are shown in Fig. 3(d). A type IV adsorption isotherm is observed for CEG with a hysteresis loop at relative pressures ranging from 0.4 to 1.0, indicating the mesoporous structure. The BET-specific surface area (BET-SSA) of CEG was obtained to be 72.2 $m^2 g^{-1}$, whereas the BET-SSA of the starting natural flake graphite was 8.5 $m^2 g^{-1}$. In addition, the CEG showed a greater SSA value than that of CrO_3-CEG (58.4 $m^2 g^{-1}$), indicating the existence of a better chemical expansion and a higher number of pores distributed in the CEG structure. The corresponding pore-size distribution curve (Fig. 3(e)) derived from the BJH method showed that most of the pores are distributed in the range of 2-50 nm with an approximate diameter of 3.07 nm, confirming the existence of mesopores in the structure.

Fig. 3(f) displays the FTIR spectrum of as-prepared CEG. The absorption peaks at 2,850 and 2,920 cm^{-1} belong to the symmetric and asymmetric vibration of CH_2, which are possibly due to the oxidation of graphite. The absorption peak at 1,745 cm^{-1} is assigned to stretching vibrations of C=O. The peak at 1,654 cm^{-1} is ascribed to the C=C stretching vibration, indicating that carbon atoms with sp^2 hybridization are still tightly arranged in a lattice of hexagonal rings. The characteristic peaks at 1,125 and 1,045 cm^{-1} are attributed to the stretching vibrations of C-O. The presence of some oxygen-containing groups in the structure originated from

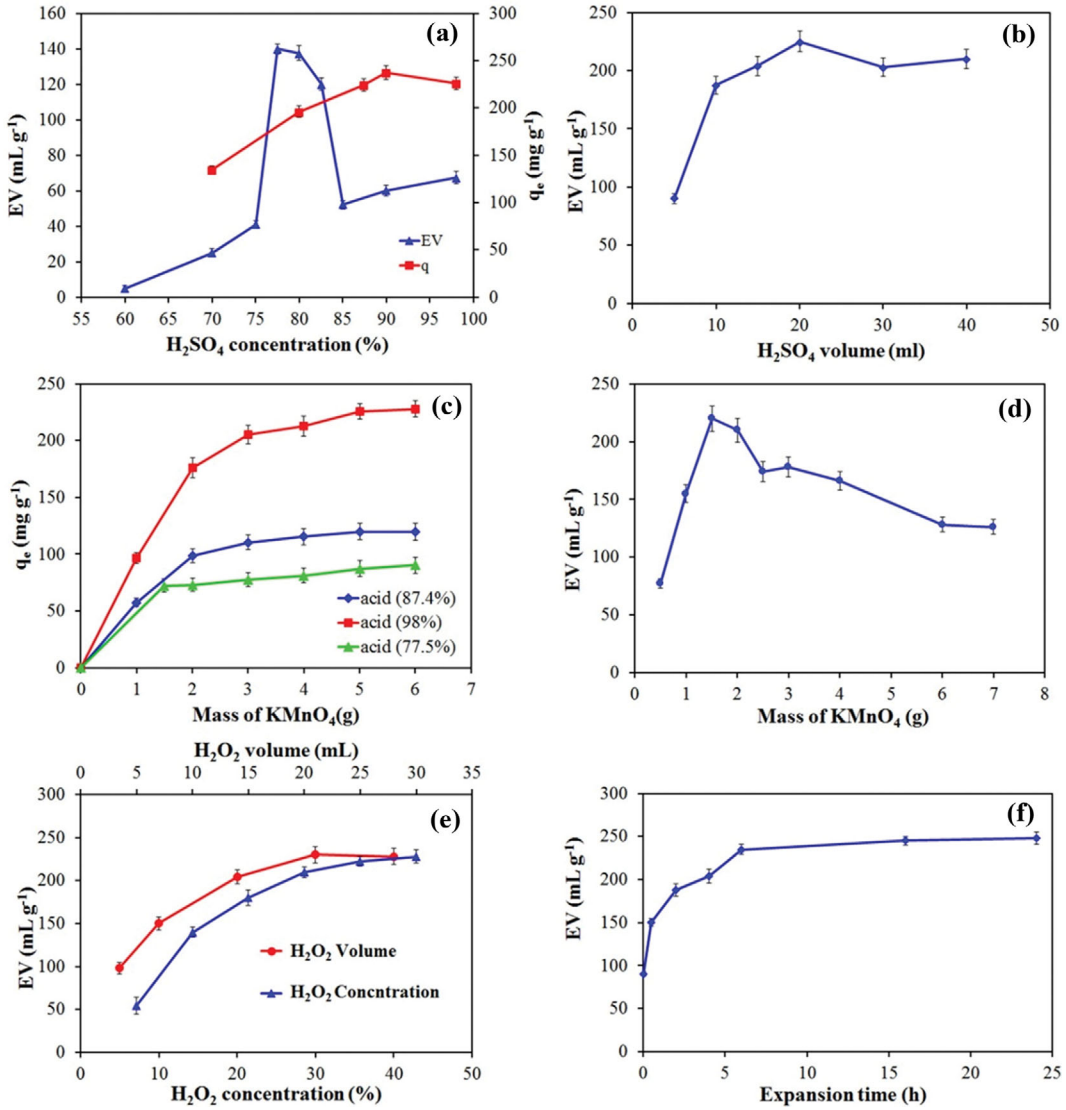

Fig. 4. The effect of (a) sulfuric acid concentration on the EV and MB adsorption capacity; (b) H_2SO_4 volume on the EV (c) $KMnO_4$ dosage at various acid concentrations on the MB adsorption capacity; (d) $KMnO_4$ dosage on the EV; (e) H_2O_2 volume and H_2O_2 concentration on the EV; and (f) the reaction time on the EV.

the graphite oxidation by $KMnO_4$.

3. Effective Parameters in the Expansion of Graphite

The expanded volume (EV) was used to study the efficiency of the graphite expansion. To obtain the best performance for graphite expansion, the effect of different parameters on the EV, including sulfuric acid mass concentration and amount, $KMnO_4$ dosage, hydrogen peroxide concentration, and the reaction time, were investigated and optimized.

3-1. Effect of Sulfuric Acid Concentration on Expansion and Adsorption of MB

The effect of H_2SO_4 mass concentration on the graphite expansion was studied at different concentrations in the range of 60-98 wt% (Fig. 4(a)). For this purpose, before the reaction, the concentrated H_2SO_4 (98 wt%) was diluted with deionized water to the desired concentration. It was found that the EV was increased by increasing of H_2SO_4 concentration from 60 to 77.5 wt%, and when the concentration reached 77.5 wt%, the maximum EV of 140 $mL \cdot g^{-1}$ could be obtained. But at higher H_2SO_4 concentration, it acts as an oxidant, and excessive oxygenation of the graphite plane can lead to a decrease in the EV. Thus, the optimum concentration of H_2SO_4 was set at 77.5 wt%.

The adsorption of MB on the surface of the CEG was also investigated at different acid concentrations (Fig. 4(a)). MB is a cationic dye that contains aromatic rings, thereby making this material to be adsorbed on the CEG surface through π-π stacking and electrostatic interactions. At low concentrations of acid, a small number of oxygen-containing groups would exist at the CEG structure. Thus, MB can initially diffuse through the CEG pores and adsorbed by it via π-π stacking interactions. With increasing acid concentration, the surface of the CEG will be more negatively charged in the solution due to introducing greater amount of oxygen-containing groups in the structure. Thus, besides the π-π stacking, the positively charged MB was attracted strongly by the negatively charged CEG via the electrostatic attraction, which would lead to an increase in the adsorption capacity.

3-2. Effect of the amount of Sulfuric Acid on Expansion

Sulfuric acid plays different roles in the expansion reaction in this work: as an intercalating agent, as an oxidant, and as an acidic medium to provide the oxidation of graphite with $KMnO_4$. As shown in Fig. 4(b), the expansion volume of EG first increased with increasing the amount of H_2SO_4 77.5 wt%, and then it slowly decreased at higher amounts. When the amount of sulfuric acid was 20 mL, a large expandable volume of 225 $mL \cdot g^{-1}$ was achieved. Sulfuric acid first acted as an acid to provide an acidic medium for the reaction with $KMnO_4$. Insufficient H_2SO_4 leads to incomplete interaction with $KMnO_4$ to act as an intercalating agent inserted between the graphite layers. With increasing in H_2SO_4 dosage, the formation of active species of Mn_2O_7 is enhanced, causing a better intercalation reaction and the increase of EV. However, when the amount of acid is excessive, it acts as an acid and oxidizes the graphite, which causes critical damage to the structure of graphite. In addition, at excess amount of acid, the reaction media is diluted, and the amount of $KMnO_4$ diffused to the graphite interlayers per unit time is limited. Thus, more H_2SO_4 molecules are buried between the layers instead of Mn_2O_7 molecules acting as an intercalating agent (Eq. (5)), which results in the reduction of EV.

$$5C+KMnO_4+17H_2SO_4 \rightarrow 5C^+ \cdot HSO_4^- + 2H_2SO_4 + MnSO_4 + KSO_4 + 4H_2O \quad (5)$$

3-3. Effect of Potassium Permanganate Dosage on the Mb Adsorption

The effect of $KMnO_4$ dosage on the adsorption of MB at various acid concentration is shown in Fig. 4(c). As can be seen, by increasing the amount of $KMnO_4$, the adsorption capacity of MB increases. This is due to the existence of more active sites on the adsorbent at higher dosage of $KMnO_4$. Moerover, at higher acid concentration, higher adsorption is achieved, which is a result of better intercalation reaction and therefore existence of more active sites on the adsorbent.

3-4. Effect of the amount of Potassium Permanganate on Expansion

The amount of $KMnO_4$ has an important effect on the EV. The results (Fig. 4(d)) demonstrate that the EV first increases along with the increase of the $KMnO_4$ amount to 1.5 g and then decreases by further increasing the $KMnO_4$ dosage. With an insufficient amount of $KMnO_4$, the amount of intercalating agent getting into the interlayer is low, and thus the O_2 gas evolution is limited, which leads to the reduction of the expansion volume. On the other hand, excessive amounts of $KMnO_4$ lead to the intensive oxidation of the graphite and opening the interlayer distances too large, which results in the escape of the intercalation agent from the layers and a decrease in EV. In addition, it can oxidize the graphite layers excessively and create large defects in the structure. Based on Fig. 4(b), when the mass ratio of $KMnO_4$ to graphite is 1.5 $g \cdot g^{-1}$, the prepared EG reaches a maximum EV of 220 $mL \cdot g^{-1}$. Thus, the appropriate dosage of $KMnO_4$ was selected as 1.5 $g \cdot g^{-1}$.

3-5. Effect of Hydrogen Peroxide Concentration on Expansion

For preparing CEG, H_2O_2 has an essential role in the expansion of graphite by producing a high volume of gas through the chemical reaction with intercalating molecules. It was found that the H_2O_2 concentration has a positive correlation with the graphite EV. From Fig. 4(e), it is clear that maximum EV can be achieved with a hydrogen peroxide solution (30% wt). Increasing the H_2O_2 concentrations leads to a reaction with more intercalation species and more oxygen release, which results in higher graphite EV. Therefore, H_2O_2 30% was selected for the chemical expansion of graphite.

3-6. Effect of the amount of Hydrogen Peroxide on Expansion

The dosage of H_2O_2 also has a direct effect on the expansion volume. According to the results (Fig. 4(e)), with increasing the amount of H_2O_2 30%, the EV was increased, reached a maximum at the amount of 30 mL, and then remained constant with further increasing the volume of H_2O_2. Indeed, H_2O_2 plays two main roles in the whole reaction: (1) evolving oxygen gas by the chemical reaction with the intercalating molecules, which is helpful for increasing the EV of the expandable graphite (see Eq. (4)), and (2) removing ash by interaction with MnO_2 and excess MnO^{4-} and converting them into Mn^{2+}, which would be washed away more easily (Eq. (6) and Eq. (7)):

$$MnO_2 + H_2O_2 + 2H^+ \rightarrow Mn^{2+} + \uparrow O_2 + 2H_2O \quad (6)$$

$$2MnO_4^- + 5H_2O_2 + 6H^+ \rightarrow 2Mn^{2+} + \uparrow 5O_2 + 8H_2O \quad (7)$$

3-7. Effect of Expansion Time

As shown in Fig. 4(f), with increasing the expansion time, the EV increased rapidly and after the reaction time of 6 h, it reached

Table 1. Comparison of the EV of the synthesized CEG with other reported EG

Starting materials	Temperature (°C)	EV (mL/g)	Ref.
Flake graphite (320 μm); CH_3COOH and $HClO_4$ (intercalator), $K_2Cr_2O_7$ (oxidant)	1,000	400	[32]
Graphite flake (≤160 μm), Acetic anhydride (intercalator), $K_2Cr_2O_7$ (oxidant)	1,000	60	[38]
Natural flake graphite (0.3 mm), $KMnO_4$ (oxidant), H_2SO_4 (intercalator) and sodium tripolyphosphate (assistant intercalator)	800	630	[42]
Natural flake graphite (+50 mesh), $(NH_4)_2S_2O_8$ (intercalator) and H_2SO_4 (98%)	Room-temperature	225	[43]
Natural graphite flake (100 mesh), CrO_3 (intercalator), H_2O_2 (reactive species)	Room-temperature	-	[20]
Natural graphite flake (100 mesh), $KMnO_4$ (intercalator), H_2O_2 (reactive species)	Room-temperature	250	This work

an EV value of approximately 95% of the maximum expanded volume (250 $mL \cdot g^{-1}$). At low expansion times, the intercalation reaction is not complete, and the intercalant molecules have not enough time to diffuse between layers and interact with H_2O_2 effectively; thus, the EV will be low. The EV was then increased slightly when the time was prolonged to 24 h. Note that the overreaction times may lead to breaking the EG worms due to the superfluous expansion.

4. Comparison with other Synthesized EG

The as-synthesized CEG was compared to previously reported EGs in the literature [20,32,38,42,43]. As shown in Table 1, the expanded volume of the CEG was comparable with others. Although in some studies, higher expanded volumes were achieved, but their expansion processes were performed under applying a high temperature for the intercalated graphite [32,42]. In addition, most of the studies involved the use of toxic chemicals, such as $K_2Cr_2O_7$ and CrO_3 or could generate toxic gases such as ClO_2 (caused by ClO_4^- decomposition) during the preparation process, which is harmful to the environment and health. These limitations make these procedures hardly acceptable for the mass production of graphene. The developed method has a simple protocol with no emission of chromium into the environment, which makes it suitable for mass production of EG and graphene.

5. Adsorption Experiments

5-1. Effect of the amount of Potassium Permanganate on the Adsorption of MB

The MB adsorption on the CEG at different dosages of $KMnO_4$ showed that by increasing the mass of the $KMnO_4$, the quantity of dye adsorbed on the CEG was continuously increased (Fig. 4(c)). As described previously, the interaction between the CEG and MB is enhanced by increasing the amount of oxygen contacting groups on the structure as the negatively charged CEG upon hydrolyzing of oxygen groups in the aqueous media adsorbed cationic MB by electrostatic interactions. $KMnO_4$ is a strong oxidizing agent, and at high dosage levels, it oxidized the graphitic structure, resulting in an increase in the adsorption of MB by the adsorbent. As shown in Fig. 4(c), the acid concentration and $KMnO_4$ dosage have a correlative effect on the adsorption capacity of MB. When the amount of $KMnO_4$ is increased, a higher acid concentration leads to higher adsorption of MB. This phenomenon is more brilliant at concentrated sulfuric acid (99.8%) with a maximum MB adsorption capacity of 399.08 $mg \cdot g^{-1}$. Both sulfuric acid and $KMnO_4$ have a significant role in the oxidation of the graphite and creating many oxygen-containing groups on the CEG structure, which increases the adsorption of cationic MB.

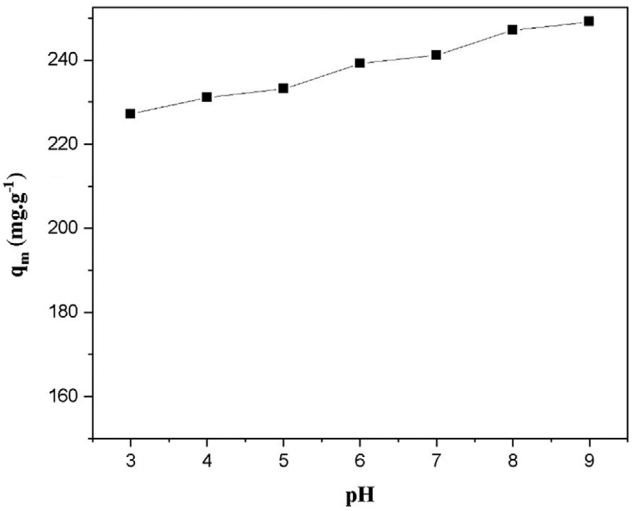

Fig. 5. Effect of pH on the adsorption of MB by CEG in room temperature.

5-2. Effect of pH

Fig. S3 shows the effect of pH on the zeta potential of CEG. As can be seen, the zeta potential of CEG has a negative value above the pH value of 5, which shows the negative surface charge of CEG at higher pH values. Effect of pH on the adsorption of MB by CEG was studied (Fig. 5). Increasing the initial pH value resulted in the increasing of adsorption capacity. This is because by increasing the pH, more functional groups are formed on the surface of CEG and therefore, a stronger electrostatic interaction is created. Moreover, as mentioned before, the surface of the CEG was negative charged above the pH value of 5 which resulted in increasing of MB adsorption.

5-3. Effect of Temperature

Fig. S4 shows the effect of temperature on the adsorption capacity of MB by CEG. The equilibrium adsorption capacity of MB on the CEg seems to slightly increase from 247.8 at 25 °C to 251.9 mg g^{-1} at 55 °C. As can be seen, MB adsorption by CEG was favored at higher temperature. However, the increase in adsorption of MB was obtained slowly at higher temperature.

5-4. Adsorption Kinetics

The adsorption of MB onto CEG showed that the adsorption

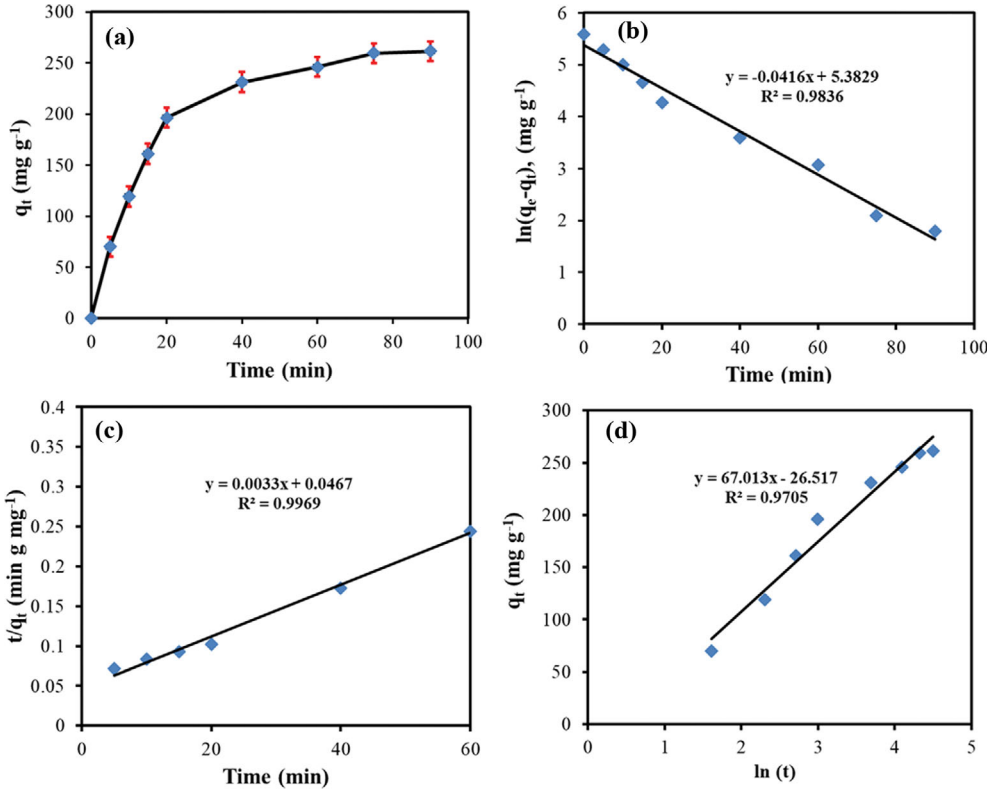

Fig. 6. (a) Effect of time on the MB adsorbed by CEG; The linear plot of (b) pseudo-first-order model; (c) pseudo-second-order model; and (d) Elovich model.

was fast initially, then gradually slowed, and finally reached equilibrium (Fig. 6). The decrease in the amount of MB adsorbed along with increasing the time may be due to the occupation of available adsorption sites by adsorbate molecules. Moreover, the surface of the CEG is negatively charged because of the oxygen containing groups and since the MB in aqueous solution has a positive charge, the adsorption of Mb on CEG takes place on the basis of electrostatic attraction. To further investigate the adsorption mechanism, the kinetic data were fitted to pseudo-first-order, pseudo-second-order, and Elovich kinetic models.

The pseudo-first-order equation is expressed as follows (Eq. (8)):

$$\ln(q_e - q_t) = \ln q_e - k_1 t \quad (8)$$

where q_t is the amount of MB adsorbed at any time (mg·g^{-1}), q_e is the amount of MB adsorbed at equilibrium point (mg·g^{-1}), k_1 is the pseudo-first-order rate constant (min^{-1}), and t is the contact time (min).

The pseudo-second-order kinetic model in the linearized form [38] is represented by the following equation:

$$\frac{t}{q_t} = \frac{1}{k_2 q_e^2} + \frac{t}{q_e} \quad (9)$$

where k_2 is the pseudo-second-order rate constant (g·mg^{-1}·min^{-1}).

The Elovich model equation is expressed as:

$$q_t = \left(\frac{1}{\beta}\right)\ln\alpha\beta + \left(\frac{1}{\beta}\right)\ln t \quad (10)$$

Table 2. Parameters of different kinetic models obtained for MB adsorption onto the CEG

Model	Parameters	Value
Pseudo-first-order	q_e (mg·g^{-1})	217.64
	K_1 (min^{-1})	0.0416
	R^2	0.9836
Pseudo-second-order	q_e (mg·g^{-1})	306.76
	K_2 (g·mg^{-1}·min^{-1})	0.0002
	R^2	0.9969
Elovich	α	44.56
	β	0.014
	R^2	0.9854

where α is the Elovich initial adsorption rate constant (mg·g^{-1}·min^{-1}), and β is the Elovich desorption constant (g·mg^{-1}).

The linear plots of kinetic models for MB adsorption onto the CEG and the corresponding kinetic parameters obtained from fitting the models are presented in Fig. 6 and Table 2. Clearly, the regression coefficient (R^2=0.9969) of the pseudo-second-order kinetic model is higher than that of pseudo-first-order (R^2=0.9836) and Elovich kinetic model (R^2=0.9705), suggesting that the kinetic modeling of MB adsorbed by the CEG follows the pseudo-second-order kinetic model.

5-5. Adsorption Isotherm

The adsorption isotherm can provide useful information about

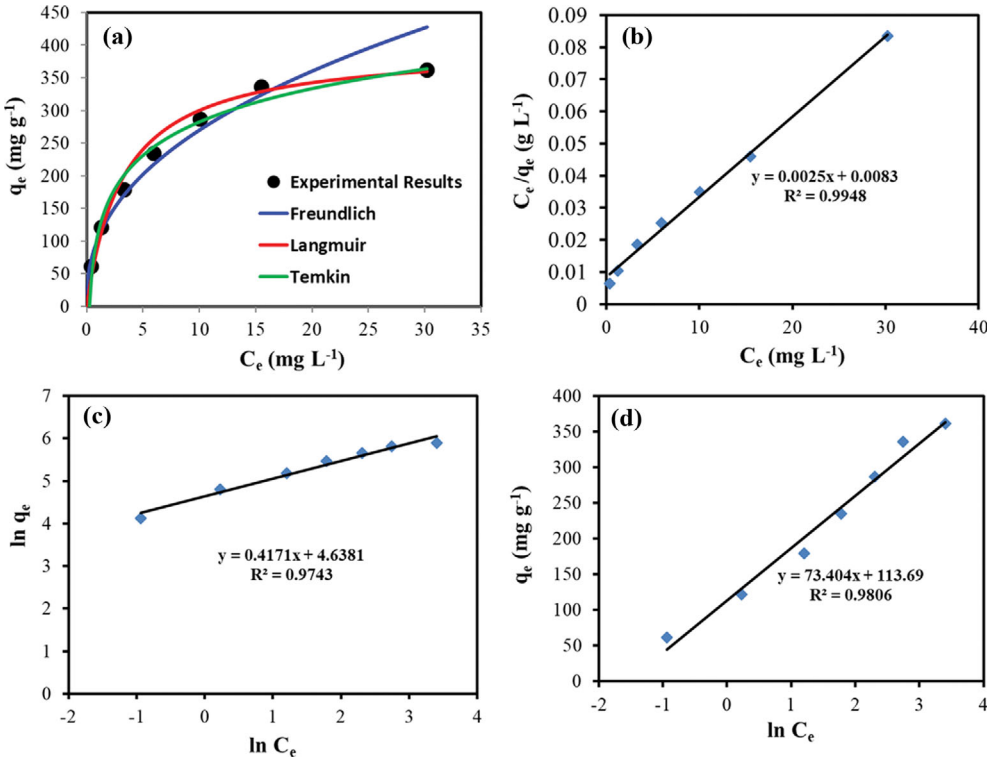

Fig. 7. (a) Equilibrium adsorption isotherms of MB adsorption onto the CEG at 25 °C; The linear plot of (b) Langmuir model; (c) Freundlich model; and (d) Temkin model.

the interaction between the adsorbate and the surface of the adsorbent at a constant temperature. Three isotherm models, the Langmuir isotherm [44], the Freundlich isotherm [45], and the Temkin isotherm [46], were used for describing the results (Fig. 7(a)). The Langmuir isotherm is based on the assumption of monolayer adsorption on a homogeneous surface [47]. The linear form of Langmuir isotherm is expressed by Eq. (11):

$$\frac{C_e}{q_e} = \frac{1}{q_m k_L} + \frac{C_e}{q_m} \tag{11}$$

where C_e is the equilibrium concentration of MB in the solution (mg·L^{-1}), q_e and q_m are the equilibrium adsorption capacity (mg·g^{-1}), and maximum adsorption capacity (mg·g^{-1}) of MB, respectively, and K_L is the Langmuir adsorption constant (L·mg^{-1}).

The Freundlich isotherm assumes that the surface of the adsorbent is heterogeneous [48]. The linear form of the Freundlich isotherm can be expressed by the following equation:

$$\ln q_e = \frac{1}{n}\ln C_e + \ln k_f \tag{12}$$

where K_f is the Freundlich adsorption constant (mg·g^{-1}) (mg·L^{-1})$^{-1/n}$, and 1/n is the heterogeneity parameter.

The Temkin isotherm assumes a linear relationship between the decrease in adsorption energy and surface coverage. The linear equation of the Temkin isotherm can be expressed as:

$$q_e = B\ln(A) + B\ln(C_e) \tag{13}$$

where B is the constant related to the heat of adsorption (J·mol^{-1}), and A is the Temkin isotherm equilibrium binding constant (L·g^{-1}).

Figs. 7(b)-(d) display the linear fitted model plots for the adsorption of MB onto the CEG. The fitting isotherm parameters and the R^2 values are presented in Table 3. According to the regression coefficients, the Langmuir isotherm (R^2=0.9926) fitted the experimental data better than the Freundlich model (R^2=0.9743) and Tempkin isotherm (R^2=0.9774), indicating the monolayer coverage of MB molecules at the surface of the adsorbent. The essential characteristics of the Langmuir equation can be expressed by the equilibrium parameter, R_L [49]:

$$R_L = \frac{1}{(1+bC_0)} \tag{14}$$

where C_0 is the initial concentration of MB (mg·L^{-1}), and K_L is the

Table 3. The parameters of adsorption isotherms obtained for MB adsorption onto the CEG

Model	Parameters	Value
Langmuir	q_m (mg·g^{-1})	399.08
	K_L (L·mg^{-1})	0.030
	R^2	0.9926
Freundlich	1/n	0.42
	K_F (mg·g^{-1}) (mg·L^{-1})$^{-1/n}$	103.35
	R^2	0.9743
Temkin	A_T (L·g^{-1})	4.71
	B	73.40
	R^2	0.9774

Table 4. Comparison of MB maximum adsorption capacity of different graphene based adsorbents

Adsorbent	Temperature (K)	Isotherm model	q_m (mg·g^{-1})	Reference
Graphene	293	Langmuir	153.85	[61]
GO with oxidation degree of 2	298	Langmuir	164.5	[62]
MGC	293	Langmuir	65.79	[63]
Graphene aerogel	-	Langmuir	332.23	[64]
This study	293	Langmuir	339.08	-

Langmuir adsorption constant (L·mg^{-1}). The R_L value indicates the adsorption to be favorable ($0<R_L<1$), linear ($R_L=1$), irreversible ($R_L=0$), or unfavorable ($R_L>1$). In this study, the value of R_L was found to be 0.016, indicating the adsorption process of MB was favorable for the prepared CEG. The adsorption capacity (399.08 mg·g^{-1}) of the adsorbent determined from the Langmuir isotherm was higher than that of many other previously reported adsorbents for MB removal [50-60], suggesting that the as-prepared CEG has great potential application in water treatment processes. Table 4 presents a comparison between the maximum adsorption capacity of various adrorbents for MB. As it can be seen, the prepared CEG has higher adsorption capacity in comparison to other graphene based adsorbent.

CONCLUSION

A simple room-temperature method based on $KMnO_4$ was developed to prepare highly expanded graphite. In this method, all processes, including intercalation and expansion, were conducted under ambient conditions. The chemical expansion of intercalated graphite in the H_2O_2 solution generated a worm-like product with a highly porous interconnected structure. By studying and optimizing the operating parameters, a high expansion volume of 250 mL·g^{-1} was achieved without any heating or high-temperature treatment. The experimental conditions of the proposed expansion method were obtained as $KMnO_4$: H_2SO_4 (77.5%) : H_2O_2 (30%)= 1.5 : 20 : 30 (g : mL : mL) as the mass ratio of graphite, intercalation time of 90 min, and expansion time of 6 h. It is expected that the developed low-temperature method for the CEG preparation may offer exciting opportunities for mass production of lightly oxidized graphene sheets. The prepared CEG was then applied as an adsorbent for MB removal from an aqueous solution. The adsorption experiments indicate that the pseudo-second-order kinetic model and Langmuir isotherm model were well fitted to the adsorption data. The results confirmed that the synthesized CEG could be used as an effective adsorbent in water treatment processes.

ACKNOWLEDGEMENTS

This work was supported by a grant provided by the School of Environment, College of Engineering, University of Tehran, Tehran, Iran.

SUPPORTING INFORMATION

Additional information as noted in the text. This information is available via the Internet at http://www.springer.com/chemistry/journal/11814.

REFERENCES

1. Y. F. Zhao, M. Xiao, S. J. Wang, X. C. Ge and Y. Z. Meng, *Compos. Sci. Technol.*, **67**, 2528 (2007).
2. D. D. L. Chung, *J. Mater. Sci.*, **51**, 554 (2015).
3. A. Lorenzetti, B. Dittrich, B. Schartel, M. Roso and M. Modesti, *J. Appl. Polym. Sci.*, **134**, 1 (2017).
4. T. Peng, B. Liu, X. Gao, L. Luo and H. Sun, *Appl. Surf. Sci.*, **444**, 800 (2018).
5. S. M. Tichapondwa, S. Tshemese and W. Mhike, *Chem. Eng. Trans.*, **70**, 847 (2018).
6. C. Xu, C. Jiao, R. Yao, A. Lin and W. Jiao, *Environ. Pollut.*, **233**, 194 (2018).
7. M. Zhao and P. Liu, *Desalination*, **249**, 331 (2009).
8. Y. Y. Zhou, S. W. Wang, K. N. Kim, J. H. Li and X. P. Yan, *Talanta*, **69**, 970 (2006).
9. F. Zhang, Q. Zhao, X. Yan, H. Li, P. Zhang, L. Wang, T. Zhou, Y. Li and L. Ding, *Food Chem.*, **197**, 943 (2016).
10. X. Ding, R. Wang, X. Zhang, Y. Zhang, S. Deng, F. Shen, X. Zhang, H. Xiao and L. Wang, *Mar. Pollut. Bull.*, **81**, 185 (2014).
11. B. Tryba, A. W. Morawski, R. J. Kaleńczuk and M. Inagaki, *Spill Sci. Technol. Bull.*, **8**, 569 (2003).
12. M. Yang, Y. Zhao, X. Sun, X. Shao and D. Li, *Desalin. Water Treat.*, **52**, 283 (2014).
13. X. Jiao, L. Zhang, Y. Qiu and Y. Yuan, *RSC Adv.*, **7**, 38350 (2017).
14. L. Jiang, J. Zhang, X. Xu, J. Zhang, H. Liu, Z. Guo, Y. Kang, Y. Li and J. Xu, *Appl. Surf. Sci.*, **357**, 2355 (2015).
15. C. Xu, W. Yang, W. Liu, H. Sun, C. Jiao and A. Lin, *J. Environ. Sci. (China)*, **67**, 14 (2018).
16. M. N. Carvallho, K. S. Da Silva, D. C. S. Sales, E. M. P. L. Freire, M. A. M. Sobrinho and M. G. Ghislandi, *Water Sci. Technol.*, **73**, 2189 (2016).
17. Y. Kong, J. Yuan, Z. Wang, S. Yao and Z. Chen, *Appl. Clay Sci.*, **46**, 358 (2009).
18. X. Y. Pang and F. Gong, *E-Journal Chem.*, **5**, 802 (2008).
19. X. Van Heerden and H. Badenhorst, *Carbon*, **88**, 173 (2015).
20. S. Lin, L. Dong, J. Zhang and H. Lu, *Chem. Mater.*, **28**, 2138 (2016).
21. A. Celzard, J. F. Mareché and G. Furdin, *Prog. Mater. Sci.*, **50**, 93 (2005).
22. I. M. Afanasov, O. N. Shornikova, D. A. Kirilenko, I. I. Vlasov, L. Zhang, J. Verbeeck, V. V. Avdeev and G. Van Tendeloo, *Carbon*, **48**, 1862 (2010).

23. L. Wu, W. Li, P. Li, S. Liao, S. Qiu, M. Chen, Y. Guo, Q. Li, C. Zhu and L. Liu, *Small*, **10**, 1421 (2014).
24. Z. Xue, S. Zhao, Z. Zhao, P. Li and J. Gao, *J. Mater. Sci.*, **51**, 4928 (2016).
25. P. He, J. Zhou, H. Tang, S. Yang, Z. Liu, X. Xie and G. Ding, *J. Colloid Interface Sci.*, **542**, 387 (2019).
26. L. Dong, Z. Chen, S. Lin, K. Wang, C. Ma and H. Lu, *Chem. Mater.*, **29**, 564 (2017).
27. Y. Chen, S. Li, R. Luo, X. Lv and X. Wang, *New Carbon Mater.*, **28**, 435 (2013).
28. J.-C. An, E. J. Lee and I. Hong, *J. Ind. Eng. Chem.*, **47**, 56 (2017).
29. A. V Melezhyk and A. G. Tkachev, *Nanosyst. Physics, Chem. Math.*, **5**, 294 (2014).
30. S. Park, J. Kim, K.-J. Jeon and S.-H. Yoon, *J. Nanosci. Nanotechnol.*, **16**, 4450 (2016).
31. N. E. Sorokina, I. V. Nikol'skaya, S. G. Ionov and V. V. Avdeev, *Russ. Chem. Bull.*, **54**, 1749 (2005).
32. J. Li, H. Da, Q. Liu and S. Liu, *Mater. Lett.*, **60**, 3927 (2006).
33. Z. Ying, X. Lin, Y. Qi and J. Luo, *Mater. Res. Bull.*, **43**, 2677 (2008).
34. Y. Lin, Z. H. Huang, X. Yu, W. Shen, Y. Zheng and F. Kang, *Electrochim. Acta*, **116**, 170 (2014).
35. W. Zhao, P. H. Tan, J. Liu and A. C. Ferrari, *J. Am. Chem. Soc.*, **133**, 5941 (2011).
36. T. Zhao, W. Jin, Y. Wang, X. Ji, H. Yan, M. Khan, Y. Jiang, A. Dang, H. Li and T. Li, *Mater. Lett.*, **212**, 1 (2018).
37. A. M. Dimiev, G. Ceriotti, A. Metzger, N. D. Kim and J. M. Tour, *ACS Nano*, **10**, 274 (2016).
38. J. H. Li, L. L. Feng and Z. X. Jia, *Mater. Lett.*, **60**, 746 (2006).
39. D. R. Dreyer, S. Park, W. Bielawski and R. S. Ruoff, *Chem. Soc. Rev.*, **39**, 228 (2010).
40. N. Kumar and V. C. Srivastava, *ACS Omega*, **3**, 10233 (2018).
41. K. N. Kudin, B. Ozbas, H. C. Schniepp, R. K. Prud'homme, I. A. Aksay and R. Car, *Nano Lett.*, **8**, 36 (2008).
42. Z. Zhai, X. Pang, R. Lin, S. Sun and M. Weng, *Asian J. Chem.*, **27**, 2971 (2015).
43. T. Liu, R. Zhang, X. Zhang, K. Liu, Y. Liu and P. Yan, *Carbon*, **119**, 544 (2017).
44. C. Rooper, M. Martin, J. Butler, D. Jones, T. Weber, C. Wilson, A. De Robertis, M. Wilkins and M. Zimmermann, *Fish. Bull.*, **110**, 317 (2012).
45. H. M. F. Freundlich, *J. Phys. Chem.*, **57**, e470 (1906).
46. M. J. Temkin and V. Pyzhev, *Acta Physicochim. URSS*, **12**, 217 (1940).
47. M. Abbasi, E. Safari, M. Baghdadi and M. Janmohammadi, *J. Water Process Eng.*, **40**, 101961 (2021).
48. M. Bagheban, A. Mohammadi, M. Baghdadi, M. Janmohammadi and M. Salimi, *J. Environ. Heal. Sci. Eng.*, **17**, 827 (2019).
49. J. Yang and K. Qiu, *Chem. Eng. J.*, **165**, 209 (2010).
50. J. Saini, V. K. Garg and R. K. Gupta, *J. Mol. Liq.*, **250**, 413 (2018).
51. M. Zhao, Z. Tang and P. Liu, *J. Hazard. Mater.*, **158**, 43 (2008).
52. P. H. Ravelonandro, D. H. Ratianarivo, C. Joannis-Cassan, A. Isambert and M. Raherimandimby, *J. Chem. Technol. Biotechnol.*, **83**, 842 (2008).
53. Y. Bulut and H. Aydin, *Desalination*, **194**, 259 (2006)
54. L. Mouni, L. Belkhiri, J. C. Bollinger, A. Bouzaza, A. Assadi, A. Tirri, F. Dahmoune, K. Madani and H. Remini, *Appl. Clay Sci.*, **153**, 38 (2018).
55. T. Huang, M. Yan, K. He, Z. Huang, G. Zeng, A. Chen, M. Peng, H. Li, L. Yuan and G. Chen, *J. Colloid Interface Sci.*, **543**, 43 (2019).
56. M. Ghaedi, M. Roosta, A. M. Ghaedi, A. Ostovan, I. Tyagi, S. Agarwal and V. K. Gupta, *Res. Chem. Intermed.*, **44**, 2929 (2018).
57. K. C. Bedin, I. P. A. F. Souza, A. L. Cazetta, L. Spessato, A. Ronix and V. C. Almeida, *J. Mol. Liq.*, **269**, 132 (2018).
58. J. Oliva, A. I. Martinez, A. I. Oliva, C. R. Garcia, A. Martinez-Luevanos, M. Garcia-Lobato, R. Ochoa-Valiente and A. Berlanga, *Appl. Surf. Sci.*, **436**, 739 (2018).
59. Z. Li, X. Tang, K. Liu, J. Huang, Q. Peng, M. Ao and Z. Huang, *J. Environ. Manage.*, **218**, 363 (2018).
60. N. Chaukura, E. C. Murimba and W. Gwenzi, *Environ. Technol. Innov.*, **8**, 132 (2017).
61. T. Liu, Y. Li, Q. Du, J. Sun, Y. Jiao, G. Yang, Z. Wang, Y. Xia, W. Zhang, K. Wang, H. Zhu and D. Wu, *Colloids Surfaces B Biointerfaces*, **90**, 197 (2012).
62. H. Yan, X. Tao, Z. Yang, K. Li, H. Yang, A. Li and R. Cheng, *J. Hazard. Mater.*, **268**, 191 (2014).
63. P. Wang, M. Cao, C. Wang, Y. Ao, J. Hou and J. Qian, *Appl. Surf. Sci.*, **290**, 116 (2014).
64. L. Jiang, Y. Wen, Z. Zhu, X. Liu and W. Shao, *Chemosphere*, **265**, 129169 (2021).